

# Modeling of UAV Tether Aerodynamics for Real-Time Simulation

Max Beffert and Andreas Zell  
 Cognitive Systems Group, University of Tübingen, Germany  
 max.beffert@uni-tuebingen.de

**Abstract**—One of the main limitations of multirotor UAVs is their short flight time due to battery constraints. A practical solution for continuous operation is to power the drone from the ground via a tether. While this approach has been demonstrated for stationary systems, scenarios with a fast-moving base vehicle or strong wind conditions require modeling the tether forces, including aerodynamic effects. In this work, we propose two complementary approaches for real-time quasi-static tether modeling with aerodynamics. The first is an analytical method based on catenary theory with a uniform drag assumption, achieving very fast solve times below 1ms. The second is a numerical method that discretizes the tether into segments and lumped masses, solving the equilibrium equations using CasADi and IPOPT. By leveraging initialization strategies, such as warm starting and analytical initialization, real-time performance was achieved with a solve time of 5ms, while allowing for flexible force formulations. Both approaches were validated in real-world tests using a load cell to measure the tether force. The results show that the analytical method provides sufficient accuracy for most tethered UAV applications with minimal computational cost, while the numerical method offers higher flexibility and physical accuracy when required. These approaches form a lightweight and extensible framework for real-time tether simulation, applicable to both offline optimization and online tasks such as simulation, control, and trajectory planning.

## I. INTRODUCTION

Multirotor drones are valuable tools in various fields, including inspection, mapping, and monitoring. However, in practice, they are limited to tasks that do not require continuous operation due to their limited flight time and battery constraints. Several approaches aim to solve this problem, for example, via autonomous landing and recharging. However, truly continuous operation can so far only be achieved by powering the drone from the ground via a tether. This method has been practically employed for many stationary base or slow-moving systems, but examples of fast-moving systems are less common [1]. Therefore, we aim to provide tools to optimize the design, modeling, and control of drones tethered to a moving ground vehicle in real-world conditions like strong wind. Our specific use case is to fly above an autonomous agricultural vehicle and detect pedestrians in the surrounding area for safety and avoidance purposes. In [2], we have looked at optimization of the tether parameters, which required a basic drag model of the system. We were able to identify the drone aerodynamics, but had to make many assumptions about the aerodynamic effects of the cable. Therefore, the goal of this work is to create a simple and easily extendable tether simulation that should run in real time and provide an estimate of tether forces acting

on the drone. The inputs of this simulation are the drone and ground vehicle position measured by GPS, an air speed estimate, and the tether length, weight, diameter, and drag coefficient. Requiring the method to run in real-time extends its usefulness from offline optimization problems to real-time applications such as simulation, control, and trajectory planning.

## II. RELATED WORK

The classical use of hanging wire modeling is in the construction of power lines and bridges [3]. These mainly focus on horizontal wires and vertical loads, so while the basics are the same, the challenges are different for tethered aerial vehicles. A field that is much closer to UAVs and has seen a lot of research in this direction is for kites and tethered airfoils for wind energy [4], [5], [6]. Knowing the tether forces is especially important in this field since these vehicles do not use active propulsion, so these forces influence the vehicle's position. Similarly, there is also some research specifically for modeling tethered multirotor UAVs [7], [8], [9].

Classically, many different methods are used to solve the tether shape and forces [10]. Some are based on classical catenary theory, for example [5], that derives the quasi-analytical static solution for a tethered kite in a wind gradient. This approach has the benefit of providing a closed-form solution, but requires using the mean drag along the whole tether length, which is not physically accurate. With a solve time of approximately 1 second, this method is not feasible for real-time applications. Another downside is the lack of flexibility, as any change in the force equations or the addition of new forces would require redoing the mathematical derivation. Other examples include [8] which measures the angle of the tether on both sides and uses a catenary model for localization and [11] which models multiple drones connected by catenary tethers.

In [6], the authors model a quasi-static elastic tether as part of a landing trajectory optimal control problem. They represent the tether as lumped masses connected via elastic segments using per-segment cross-flow drag. A rigid-body velocity field is used to compute aerodynamic and centripetal loads along the tether. The tether model is integrated into a differential-algebraic equation (DAE) formulation and solved as part of the larger trajectory optimization using CasADi [12] and IPOPT [13]. This results in a physically accurate solution, but at increased computational cost. They note initialization challenges, which they solve by first solving

a low-tension problem from a simple initial guess, then progressively increasing the target tension and solving again. They do not provide any runtime figures, but the iterative initialization approach, along with the problem size, makes it less feasible for real-time use. In [4], the authors use a similar approach to model and compare different configurations of tethered airfoils for wind energy generation.

In [7], the tether is discretized into rigid segments and lumped masses, and the Lagrange equations are derived for dynamics, using cross-flow principles for lift and drag. They explicitly model the unwinding of the tether by allowing the first segment to change its length and dynamically adding or removing segments. The advantage of this method is that it provides physically accurate aerodynamics and dynamic cable behavior in 3D; however, it exhibits some numerical instability at higher wind speeds due to Euler angle singularities. Since dynamics are modeled, a small simulation time step of 0.1ms is required. Due to the increased complexity of the problem, a segment length of 1.5m was used to achieve a reasonable simulation speed; however, this limited the resolution of the results, suggesting that the method may not be suited for real-time applications with suitable accuracy. Another downside is that the complexity of the Lagrangian formulation limits flexibility when it comes to modifying forces or adding new ones. Similarly, [9] uses discrete segments with lumped masses and finite element analysis to solve the tether shape without aerodynamics for use in maritime oil spill detection.



Fig. 1: A photo of the tethered drone showing the cable curvature.

### III. METHODS

The shape and tension of a hanging wire are the result of the differential force equations at every point along the cable. These forces include the weight of the cable, the tension

in the cable, and any additional forces like drag or lift. In the case where there is a uniform mass distribution along the cable and only gravity acts on it, the tether follows the catenary shape given by

$$a * \cosh((x - x_0)/a) + y_0 \quad (1)$$

$$a = H/w \quad (2)$$

- $(x_0, y_0)$  is the offset of the catenary
- $(x_0, y_0 + a)$  is the lowest point of the catenary (vertex)
- $a > 0$  is the shape parameter
- $H$  is the constant horizontal tension
- $w$  is the cable weight per unit length

#### A. Analytical Approach

This function is used to obtain an analytical solution by determining the parameters  $a, (x_0, y_0)$  that fulfill the constraints. We define point  $p_1 = (x_1, y_1)$  as the position of the ground vehicle and  $p_2 = (x_2, y_2)$  as the position of the drone. For simplicity, we will furthermore assume that  $y_1 < y_2$ . Both  $p_1$  and  $p_2$  must lie on the curve (3) and (4). The arc length between  $p_1$  and  $p_2$  must be equal to the wire length  $L$  (5). By minimizing the constraint functions, the parameters that result in a valid catenary are determined.

$$a * \cosh((x_1 - x_0)/a) + y_0 - y_1 = 0 \quad (3)$$

$$a * \cosh((x_2 - x_0)/a) + y_0 - y_2 = 0 \quad (4)$$

$$a * |\sinh((x_2 - x_0)/a) - \sinh((x_1 - x_0)/a)| - L = 0 \quad (5)$$

Due to the low computational complexity of solving the problem, very short solve times below 1ms (Fig. 3) were achieved by using a lightweight solver (*scipy fsolve*). It is common for numerical methods to vary greatly depending on the quality of the initialization or initial guess. In this case, the solver can sometimes struggle to find a solution, especially if the problem becomes ill-posed (when the start and end points are close horizontally). To mitigate this, multiple parameter sets (Table I) are used for the initial guess to fall back on in case the solve fails. Because of the sub-millisecond solve-time and early aborting in case of bad initialization, attempting multiple solves does not have a significant impact on the runtime.

Type	Parameter Guess $(a, x_0, y_0)$
Parabolic 1x	$(a_{par}, x_{mid}, y_1 - s_{par} - a_{par})$
Parabolic Nx	$(N * a_{par}, x_{mid}, y_1 - s_{par} - N * a_{par})$
No Sag 1x	$(a_{nosag}, x_{mid}, y_1 - a_{nosag})$
No Sag Nx	$(N * a_{nosag}, x_{mid}, y_1 - N * a_{nosag})$
Large Sag	$(L/8, x_{mid}, y_1 - L/2)$

TABLE I: Initial guesses for the analytical method based on parabolic approximation and heuristics.

Generally  $x_0$  is guessed to be at the midpoint  $x_{mid} = (x_1 + x_2)/2$  between  $x_1$  and  $x_2$ . The shape parameter  $a$  is guessed using (6), which is a parabolic approximation of the catenary based on the second-order Taylor expansion (Appendix A). The tether sag is estimated by (7).

Then  $y_0 = y_1 - s - a$  is estimated following (1) since the sag is the vertical distance from  $y_1$  to the vertex and  $y_0$  is a below that. To cover different cases, an option that assumes zero sag  $a_{nosag}$  as well as different scaling factors for  $a$  are used. There is also a heuristic guess for large sag that does not use the parabolic approximation, instead assuming that the sag is approximately half the cable length.

$$a_{par} = \frac{d_x^2}{8 * s_{par}} \quad (6)$$

$$s_{par} = \sqrt{\frac{3}{8} * d_x * (L - d_x)} \quad (7)$$

- $d_x = (x_2 - x_1)$  is the horizontal distance between  $p_1$  and  $p_2$
- $s_{par}$  is the estimated sag based on the parabolic cable length equation  $L = d_x + (8s^2)/(3d_x)$  [3]

The different initial guesses from Table I were compared on a real-world flight to determine the number of cases in which the guess produced the fastest solve time. This was done to determine the order in which the guesses should be attempted to speed up the solve by not wasting time on bad guesses. The results are listed in Table II.

Method	Percentage (%)
Parabolic 2x	42.9 %
Parabolic 1.2x	27.1 %
Large Sag	10.0 %
No Sag 1x	7.1 %
No Sag 2x	4.7 %
Parabolic 0.8x	4.7 %
Parabolic 1x	3.5 %

TABLE II: Comparison between the initial guess strategies for the analytical method from Table I. Shown is the percentage of cases in which the method produced the fastest solve time. The test was run on a real-world flight to represent the actual distribution of cases.

The current catenary formulation does not model any drag; however, in the case of real-world tethered drones, having zero airspeed is uncommon due to wind and the drone's movement. Drag can be added to the catenary model by making the simplification that the aerodynamic force acts on the whole tether equally. This means that the drag behaves like a potential field that can be combined with the potential field of the tether weight. By doing this, the resulting shape is still a catenary curve, but in a rotated coordinate system where the combined potential field points down. So by first rotating the start and end points and applying the combined force instead of just the weight, the same catenary equation can be used. Points or tension values can then be sampled in the rotated coordinate system and rotated back to produce the simulation result.

The total drag on the tether is calculated using the vertical distance between  $p_1$  and  $p_2$  to calculate the exposed area for the Rayleigh drag equation (8).

$$F_D = \frac{1}{2} * \rho * C_D * A * V^2 \quad (8)$$

This approach underestimates the drag in cases where the tether sags below the start point. To obtain an accurate solution, an initial solve is performed using the vertical distance between  $p_1$  and  $p_2$  as an estimate for the vertical length of the tether. The actual vertical length is then computed numerically and used for the next iteration until the error between the estimated and actual vertical length used to calculate the drag converges. This ensures that the total amount of drag on the tether is correct.

In conclusion, the analytical model makes the assumptions of an inextensible cable without stretch, uniform drag, and a uniform mass distribution along the tether.

### B. Numerical Approach

In reality, the drag on the cable is not uniform. To achieve a physically accurate solution, it is necessary to include varying forces along the tether length. The analytical approach does not allow this since the resulting shape will not be a catenary. Therefore, we use CasADI [12], which allows defining nonlinear optimization problems symbolically and uses IPOPT [13] to solve them. For this numerical approach, the cable is split into discrete point masses connected via rigid segments. Since quasi-static equilibrium with uniform airflow direction is assumed, the tether will remain in a single vertical plane, allowing for a 2D formulation.

One way to define the problem would be to minimize the energy in the system while maintaining the length and endpoints. The downside of this approach is that it makes it harder to implement arbitrary forces, as they would have to be converted into energy, which would depend on the deflection from the rest state. Instead, a more practical approach is to redefine the problem in terms of constraint satisfaction, without requiring minimization. In this case, the positions and tension are solved directly so that the net force at each node is zero. Since an inextensible tether is assumed, the tension forces can be solved directly, in contrast to classical spring mass models. However, without a spring force to balance segment lengths, an explicit segment length constraint is necessary. By limiting the tension to positive values, the numerical stability is improved, and physically accurate solutions are ensured. This is necessary, as cables can only act in tension, not compression.

First, the segment forces are calculated by combining the drag and tension from the solver. The drag in this case is still based on the Rayleigh drag equation (8), but accurately uses the vertical length of each segment to calculate the exposed area.

$$A_{exp} = d * \Delta y \quad (9)$$

- $A$  is the area exposed to the airflow
- $d$  is the tether diameter
- $\Delta y$  is the segment vertical component (assuming horizontal wind)

At this point, other segment forces like lift or drag based on a wind gradient could be added. The forces on each node

are then summed up with a half contribution from each connected segment, plus gravity and potentially any other node-based forces like inertia. A constraint is then generated for each node to achieve zero net force.

These constraints are implemented symbolically using CasADi, which constructs the Lagrangian, applies automatic differentiation to compute the objective function gradient, constraint Jacobian, and Lagrangian Hessian, then solves the optimization problem using IPOPT. The objective function in our case is set to zero since the physics are formulated as a pure constraint satisfaction problem. The key to achieving fast solve times is to cache and reuse the CasADi solver, so the problem setup and automatic differentiation do not have to be repeated and only need to be numerically evaluated for each solve.

One inherent limitation of any discrete approach is that the segment length limits the maximum bend radius (Fig. 2). This becomes apparent when the airspeed is low and the start and end are close together horizontally, resulting in a sharp bend at the bottom. The numerical approach will still produce a result, but the forces will not be physically accurate. Therefore, it is better to use the analytical method if the horizontal distance between the start and end points is shorter than twice the segment length. By doing this check in the rotated coordinate system (as described in the analytical approach), cases with low sag and therefore without a sharp bend are handled correctly.

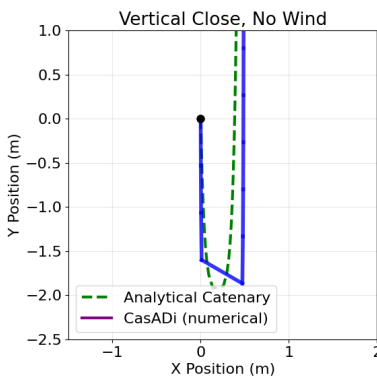


Fig. 2: Example where the start and end points are almost vertical and there is no wind. The fixed segment length of the discrete approach limits the minimum bend radius.

As previously mentioned, initialization has a significant impact on numerical methods; the same is true for this approach. Unlike the analytical method, it converges even with bad initialization, but the solve time can vary significantly. To make sure the best possible initialization is used, there are two options: using the analytical solution for initialization and using the solution from the previous time step (warm start). When using the analytical solution, it is crucial to sample the points at equal arc lengths instead of just uniformly along the x-axis. The same applies to calculating the tensions where the segment midpoints need to be sampled.

Compared to the analytical method, fewer assumptions need to be made since any arbitrary force could be added according to the decision diagram in (Appendix B), to make the simulation mode accurate. However, it has to be tested if the solver is stable for a specific arbitrary force.

#### IV. EXPERIMENTS AND RESULTS

Figure 4 shows the tether shape and tension along the tether for different configurations. It also highlights that the analytical solution is very close to the numerical one in most cases. Another interesting insight from the plots is that the forces can exceed the tether weight by a large margin if there is strong wind and the tether gets tight 4c. This case could be detected on the ground by measuring the angle of the tether; the steeper it is, the bigger the expected tension. In this case, the forces should be lowered by decreasing the drone's altitude. The comparison between 4d and 4e, 4f show that there are some differences between the analytical and numerical solution in cases with large horizontal distance and strong winds. This is due to the uniform drag assumption of the analytical approach, which becomes apparent when there are more almost horizontal segments.

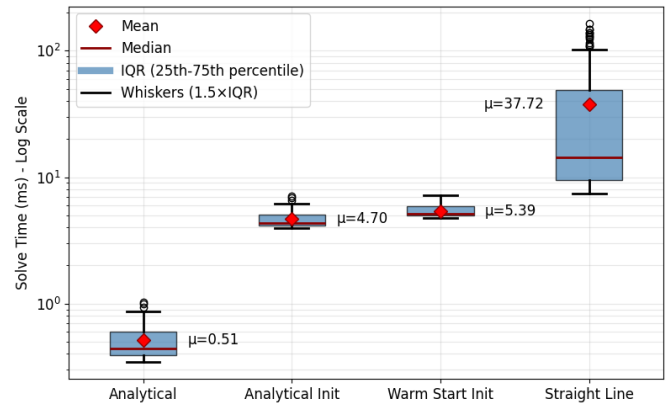


Fig. 3: Comparison of solve times for the analytical approach, numerical approach with analytical initialization, numerical approach with warm start, and the numerical approach initialized with a straight line. The time to calculate the numerical initialization is not included. Note that the y-axis is on a logarithmic scale. The numerical method was run for 60 segments. It shows that the numerical approach is roughly 10 times slower than the analytical one, and using unsuitable initialization can further increase the solve time by a factor of 8.

Figure 3 has the solve times for a real-world flight. It shows that the analytical method is very fast, with a mean runtime of 0.51ms, even with the iterative approach and using multiple guesses. This makes it feasible to use the analytical solution to initialize the numerical solver without a significant impact on the solve time. In this case, the mean is 4.70ms (in addition to the time necessary to calculate the analytical initialization). In case the solution from the previous time-step is used to initialize the numerical approach, the runtime is similarly fast at a mean of 5.39ms. In contrast, using a bad initialization, for example, just a straight line between start and end point, has a significant impact on the

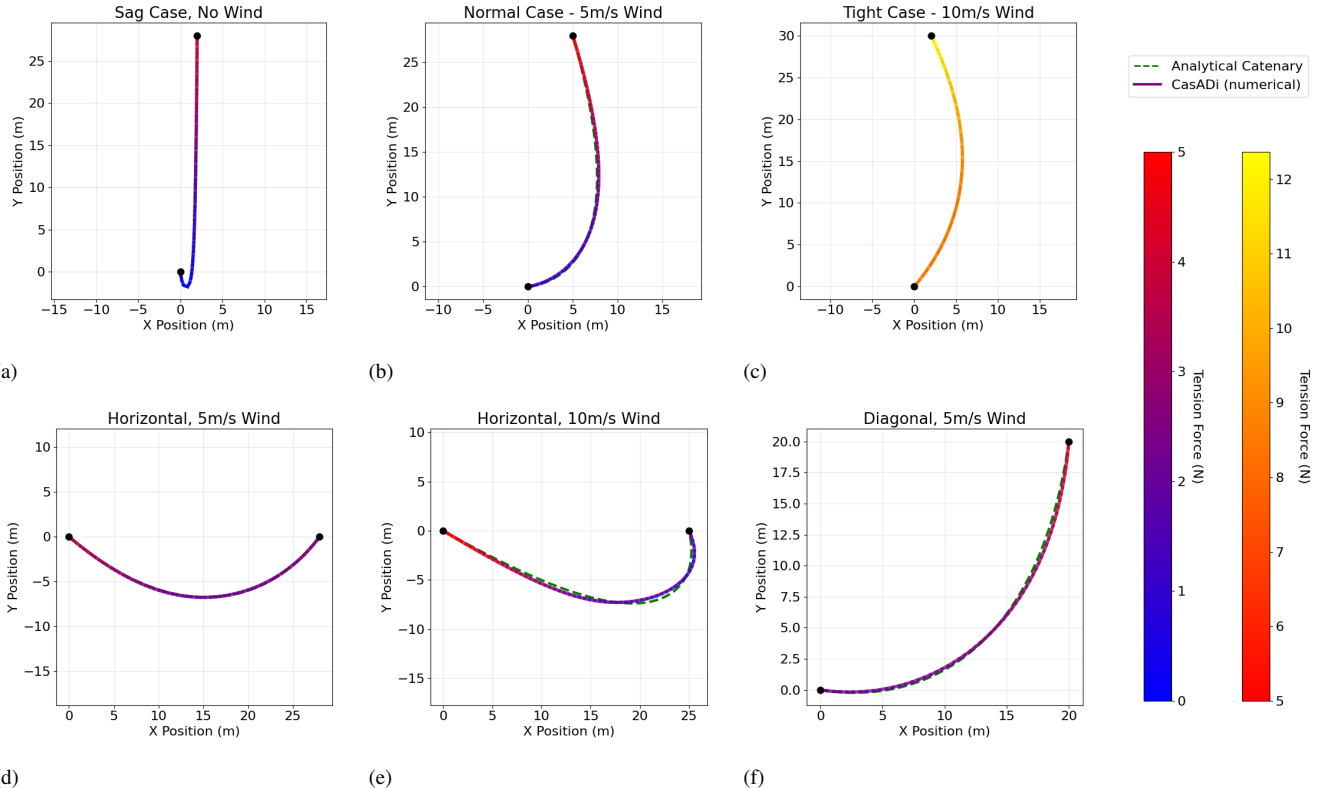


Fig. 4: Examples of the shape and tension of different configurations solved via the analytical and numerical (CasADI) approach. 4a and 4b show typical cable behaviour for a tethered UAV, while 4c highlights the high forces on tight cables. The comparison between 4d and 4e, 4f highlight that the analytical solution is less accurate for large horizontal distances and strong winds. Note that the color bars are scaled differently.

solve time, with a mean of 37.72ms and a wide distribution of values. In summary, the numerical method is about 10 times slower than the analytical one, and improper initialization can further increase the numerical solve time by a factor of 8.

Besides setting  $ipopt.tol$  and  $ipopt.constr_viol_tol$  to  $1 \times 10^{-8}$  to match the desired residual threshold of the analytical method, default solver settings were used. With some tuning of the IPOPT settings, it might be possible to further improve the solve times of the numerical approach.

To confirm the simulation results, a sensor was built to measure the tension in the cable on the drone side. It uses an inline load cell rated for 10kg, a NAU7802 analog-digital converter, and an RP2040 microcontroller (Fig. 8). The tension is measured at a rate of 10Hz and sent to the drone flight controller via MAVLink, where it is logged.

A test flight was conducted with an aluminium cable with a length of 32m and a mass of 450g at a flight height of 30m. The drone velocity was used as air speed, assuming low wind. The results of this test flight are in Fig. 5 and demonstrate excellent agreement between the analytical and numerical solutions, with the lines visually indistinguishable in the plot. The load cell measurements are in the same order of magnitude as the simulation, proving its general correctness. However, some deviations can be attributed to unexpected wind and the limited accuracy of GPS, especially regarding altitude measurements. When the

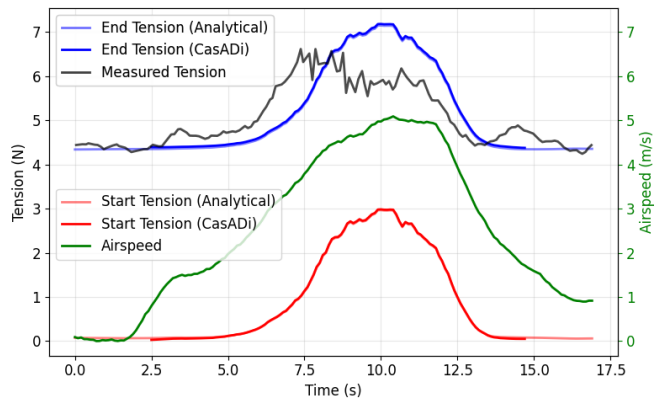


Fig. 5: Comparison between the tension from the analytical and numerical (CasADI) method on GPS data from a real flight. Start force (red) on the ground, end force (blue) on the drone. The tension was measured on the drone (black). The airspeed is shown in green. It demonstrates close agreement between the analytical and numerical method. The measurements are in the same order of magnitude but show some discrepancies due to system dynamics and GPS accuracy.

tether is almost tight, small changes in altitude can strongly affect the tension, so any mismatch between measured and actual altitude will impact the estimated tension accuracy. Additionally, the drag coefficient is assumed to be 1.2, which

is a commonly used value, but may differ in reality. We can also observe a discrepancy due to the dynamic behavior of the cable, which causes more tension during acceleration and less during deceleration. Since the proposed methods do not model dynamic behaviour, this is expected and would be less apparent during extended flight at constant velocity.

For the same flight recording, Fig. 6 shows that the difference in forces between the analytical and numerical solution is in the range of 0.04N, which is less than 1% of the total force. In most tethered drone cases the ratio between vertical and horizontal distance is high. Therefore, especially if the fastest solve time is desired, the analytical solution by itself is sufficient.

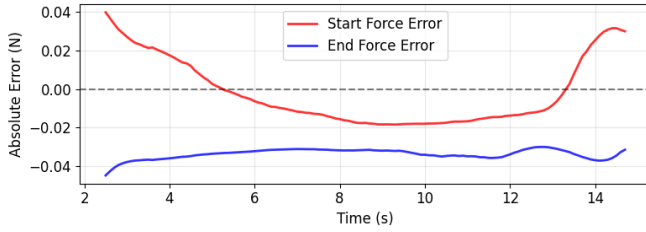


Fig. 6: The difference between the analytical and numerical tension at the start point/ground (red) and end point/drone (blue) for a real flight. It shows that the error caused by the uniform drag assumption of the analytical approach is low.

To demonstrate the flexibility of the approach and as an attempt to model some of the system dynamics, we implemented a simplified inertia force. Instead of calculating the velocities and accelerations of individual nodes, we use the acceleration of the drone to calculate the inertial forces for the whole tether. The only implementation change necessary to accomplish this was passing the acceleration into the solver and using it to calculate the inertial force from the node mass. Besides the necessary interface changes, two new lines of code were added and two lines were adjusted, showing the flexibility of the approach. Indeed, the results with the added dynamics more closely match the measured tension (Fig. 7).

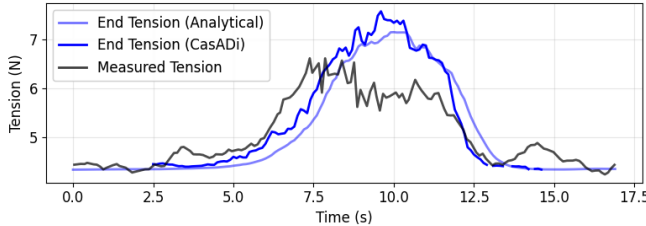


Fig. 7: Adding a simplified inertial term to the numerical (CasADI) solution shows improved physical accuracy in transient cases compared to the analytical solution without dynamics.

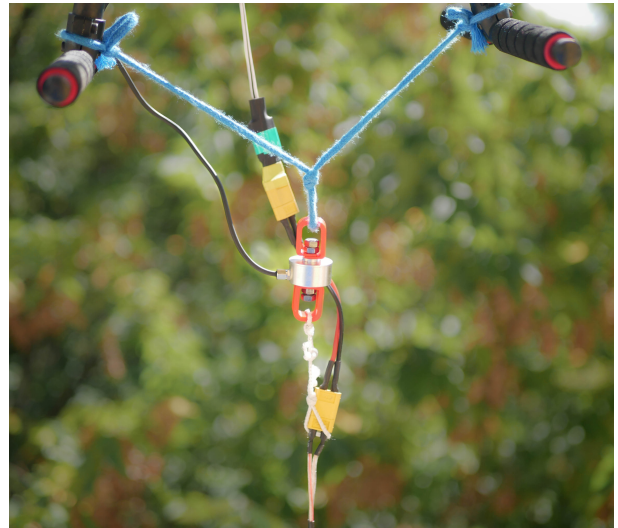


Fig. 8: Photo of the load cell sensor attached to the drone for measuring the tether tension.

## V. CONCLUSION

In this work, two complementary approaches for quasi-static real-time tether simulation with aerodynamics have been proposed. An analytical method based on catenary theory with uniform drag assumptions that achieves very fast solve times with a mean of 0.51ms, making it well-suited for real-time applications. It was shown that for typical tethered UAV cases, the error compared to more physically accurate models is below 1% of the total force, making it suitably accurate.

We also proposed a numerical approach for cases where higher accuracy is desired, using CasADI to solve a discretized version of the problem with lumped masses and rigid segments. By using either warm start or analytical initialization, it was shown that short solve times of 5ms can be achieved with this method. An additional strength of this method is that it is flexible in allowing the modification of force equations or even adding new forces to the simulation.

Real-world measurements with a load cell were used to show the general correctness of both approaches. However, GPS altitude accuracy and the quasi-static assumption led to discrepancies between the simulation and real-world measurements in transient situations.

The proposed methods successfully achieve the goal of having a flexible framework for tether simulation with real-time capabilities, making it applicable not only to offline optimization but also to real-time problems such as simulation, control, and trajectory planning. Future work could aim to reintroduce some of the system dynamics to enhance accuracy in transient situations while maintaining the fast solve speed.

In conclusion, this work strikes a balance between complexity and flexibility, as well as accuracy and real-time capabilities, making it suitable for a wide range of real-world applications such as our tethered agricultural person detection system.

## APPENDIX

### A. Derivation of (7):

$$\begin{aligned}\cosh x &= 1 + \frac{x^2}{2!} + \frac{x^4}{4!} + \dots \\ y(x) &= a * \cosh \frac{x}{a} \\ &\approx a * \left(1 + \frac{(x/a)^2}{2}\right) \\ &= a + \frac{x^2}{2a}\end{aligned}$$

This is the parabolic approximation around the vertex. For a symmetric catenary the sag  $s$  is the distance between the vertex at  $y_0 + a = a$  and start point at  $y(d_x/2)$ .

$$\begin{aligned}s &= y(d_x/2) - a \\ &\approx \frac{(d_x/2)^2}{2a} \\ a &\approx \frac{(d_x/2)^2}{2s} = \frac{d_x^2}{8s}\end{aligned}$$

### B. Additional Figures

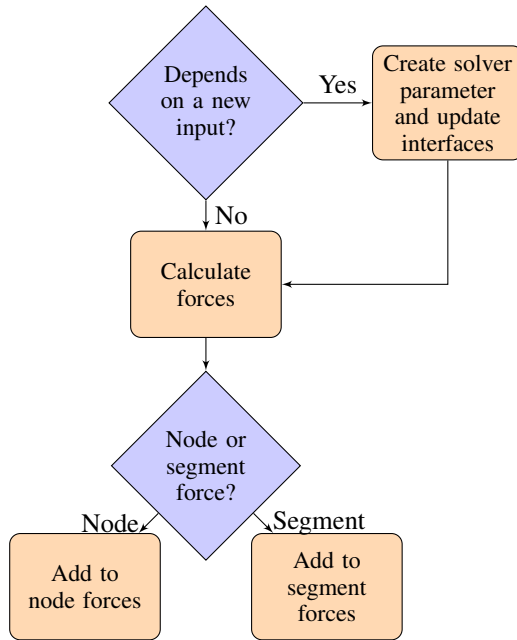


Fig. 9: Decision diagram when adding new forces to the simulation. It shows the system's flexibility, allowing for easy modifications.

## REFERENCES

- [1] M. N. Marques, S. A. Magalhães, F. N. Dos Santos, and H. S. Mendonça, "Tethered Unmanned Aerial Vehicles—A Systematic Review," *Robotics*, vol. 12, no. 4, p. 117, Aug. 2023. [Online]. Available: <https://www.mdpi.com/2218-6581/12/4/117>
- [2] M. Beffert and A. Zell, "Cable Optimization and Drag Estimation for Tether-Powered Multirotor UAVs," in *2025 International Conference on Unmanned Aircraft Systems (ICUAS)*, May 2025, pp. 15–21, iSSN: 2575-7296. [Online]. Available: <https://ieeexplore.ieee.org/document/11007916>
- [3] H. M. Irvine, *Cable Structures*. Dover Publications, 1992.
- [4] M. Zanon, S. Gros, J. Meyers, and M. Diehl, "Airborne Wind Energy: Airfoil-Airmass Interaction," *IFAC Proceedings Volumes*, vol. 47, no. 3, pp. 5814–5819, Jan. 2014. [Online]. Available: <https://www.sciencedirect.com/science/article/pii/S1474667016425218>
- [5] N. Bigi, A. Nême, K. Roncin, J.-B. Leroux, G. Bles, C. Jochum, and Y. Parlier, "Analytical Tether Model for Static Kite Flight," in *Airborne Wind Energy*, R. Schmehl, Ed. Singapore: Springer Singapore, 2018, pp. 57–78, series Title: Green Energy and Technology. [Online]. Available: [http://link.springer.com/10.1007/978-981-10-1947-0\\_3](http://link.springer.com/10.1007/978-981-10-1947-0_3)
- [6] J. Koenemann, P. Williams, S. Sieberling, and M. Diehl, "Modeling of an airborne wind energy system with a flexible tether model for the optimization of landing trajectories," *IFAC-PapersOnLine*, vol. 50, no. 1, pp. 11944–11950, Jul. 2017. [Online]. Available: <https://www.sciencedirect.com/science/article/pii/S2405896317315227>
- [7] E. Dicembrini, M. Scanavino, F. Dabbene, and G. Guglieri, "Modelling and simulation of a tethered UAS," in *2020 International Conference on Unmanned Aircraft Systems (ICUAS)*. Athens, Greece: IEEE, Sep. 2020, pp. 1801–1808. [Online]. Available: <https://ieeexplore.ieee.org/document/9214006>
- [8] A. Borgese, D. C. Guastella, G. Sutera, and G. Muscato, "Tether-Based Localization for Cooperative Ground and Aerial Vehicles," *IEEE Robotics and Automation Letters*, vol. 7, no. 3, pp. 8162–8169, Jul. 2022. [Online]. Available: <https://ieeexplore.ieee.org/abstract/document/9811264>
- [9] F. Muttin, "Umbilical deployment modeling for tethered UAV detecting oil pollution from ship," *Applied Ocean Research*, vol. 33, no. 4, pp. 332–343, Oct. 2011. [Online]. Available: <https://linkinghub.elsevier.com/retrieve/pii/S0141118711000526>
- [10] F. Fattori and S. Cocuzza, "Tethered Drones: A Comprehensive Review of Technologies, Challenges, and Applications," *Drones*, vol. 9, no. 6, p. 425, Jun. 2025, publisher: Multidisciplinary Digital Publishing Institute. [Online]. Available: <https://www.mdpi.com/2504-446X/9/6/425>
- [11] "Tethered Power for a Series of Quadcopters: Analysis and Applications." [Online]. Available: <https://arxiv.labs.arxiv.org/html/2203.08180>
- [12] J. Andersson, J. Åkesson, and M. Diehl, "CasADi: A Symbolic Package for Automatic Differentiation and Optimal Control," in *Recent Advances in Algorithmic Differentiation*, S. Forth, P. Hovland, E. Phipps, J. Utke, and A. Walther, Eds. Berlin, Heidelberg: Springer, 2012, pp. 297–307.
- [13] A. Wächter and L. T. Biegler, "On the implementation of an interior-point filter line-search algorithm for large-scale nonlinear programming," *Mathematical Programming*, vol. 106, no. 1, pp. 25–57, Mar. 2006. [Online]. Available: <https://doi.org/10.1007/s10107-004-0559-y>